Supporting Information:

Magnetic Skyrmion Formation at Lattice Defects and Grain Boundaries Studied by Quantitative Off-Axis Electron Holography

Zi-An Li[1,2,3], Fengshan Zheng[2], Amir Hossein Tavabi[2], Jan Caron[2], Chiming Jin[4], Haifeng Du[4], András Kovács[2], Mingliang Tian[4], Michael Farle[1] and Rafal E. Dunin-Borkowski[2]

[1]Faculty of Physics and Center for Nanointegration (CENIDE), University of Duisburg-Essen, 47057 Duisburg, Germany

[2]Ernst Ruska-Centre for Microscopy and Spectroscopy with Electrons and Peter Grünberg Institute, Forschungszentrum Jülich, 52425 Jülich, Germany

[3]Institute of Physics, Chinese Academy of Sciences, Beijing 100190, China

[4]High Magnetic Field Laboratory, Chinese Academy of Sciences, 230031 Anhui, China

[5]Center for Functionalized Magnetic Materials (FunMagMa), Immanuel Kant Baltic Federal University, Kaliningrad, Russian Federation

January 31, 2017

1 Note 1: Lorentz microscopy

The Fresnel (defocus) imaging mode of Lorentz microscopy is widely used for magnetic contrast analysis in the transmission electron microscope. When traversing a thin specimen that has uniform in-plane magnetic induction $\mathbf{B}$ and thickness t, an incident electron beam experiences a Lorentz force $F_L = -ev \times \mathbf{B}$ and is deflected by an angle $\theta_L = \frac{e\lambda}{h}\mathbf{B}t$ relative to the incident direction, where e is the electron charge, v is the velocity and λ is the wavelength of the incident electrons, and h is Planck's constant . The recorded magnetic contrast is related not only to local variations in in-plane magnetic induction $\mathbf{B}$ and specimen thickness t, but also to the chosen defocus value. For illustrative purposes, Figure S5 shows a simplified ray diagram that describes the concept of Fresnel imaging for a thin magnetic slab that contains oppositely magnetized domains. In focus, no magnetic contrast is seen (Fig. S5(b)). Out of focus (Fig. S5(a) and (c)), magnetically deflected electrons either converge or diverge in the image plane, resulting in dark or bright contrast of magnetic origin along the lengths of domain walls in over-focus and under-focus images. It should be noted that only in-plane components of $\mathbf{B}$ contribute to the magnetic contrast, and that specimens are normally observed in magnetic-field-free conditions with the objective lens switched off, or alternatively in a known (pre-calibrated) externally applied magnetic field.

In order to study magnetization dynamics, external stimuli can be applied to specimens during Lorentz microscopy observations. In the present study, a liquid nitrogen cooled specimen holder (Gatan, Inc.) was used to vary the specimen temperature between 95 and 370 K. The conventional microscope objective lens was used to apply magnetic fields of between 0 and 1.5 T normal to the specimen plane.

2 Note 2: Quantitative off-axis electron holography

2.1 Basis of off-axis EH

According to the Aharonov-Bohm (A-B) effect in quantum mechanics, the wavefunction of an electrically charged particle is affected by the electromagnetic potential through which it traverses. In the TEM, the phase shift of an electron wave that traverses an electron-transparent specimen (written in one dimension here for simplicity) can be expressed in the form

$$\varphi_{EM}(x) = \varphi_E + \varphi_M = C_E \int V(x,z)\,dz - 2\pi\frac{e}{h}\iint B_\perp(x,z)\,dxdz \qquad (1)$$

where x is a direction in the specimen plane, z is the incident electron beam direction, C_E is an interaction constant that takes a value of $6.53\times10^6\,rad\cdot m^{-1}$ at a microscope accelerating voltage of $300\,kV$, V is the electrostatic potential of the specimen and $B_\perp$

is the in-plane component of the magnetic induction within and around the specimen. The total recorded phase shift φ_{EM} is the sum of an electrostatic contribution to the phase shift φ_E originating from the electrostatic potential $V(r)$ (see Fig. S6(a)) and a magnetic contribution to the phase shift φ_M (see Fig. S6(b)).

One of the most widely used techniques for recording the total phase shift φ_{EM} within and around a specimen directly is the TEM mode of off-axis electron holography. The technique requires a highly coherent field-emission gun (FEG) electron source to examine a specimen, in which the region of interest is positioned so that it occupies approximately half the field of view. The application of a voltage to an electron biprism results in overlap of part of the electron wave that has passed through vacuum alone with part of the same electron wave that has passed through the specimen, as shown schematically in Fig. S6(c). If the electron source is sufficiently coherent, then an interference fringe pattern (an electron hologram) is formed in the overlap region, in addition to an image of the specimen. The amplitude and phase shift of the specimen wave are encoded in the intensity and position, respectively, of the interference fringes. For studies of magnetic materials, just as for Fresnel imaging (see above) a Lorentz lens (a high-strength minilens) allows the microscope to be operated at high magnification with the objective lens switched off and the sample located in magnetic-field-free conditions.

2.2 Separation of electrostatic and magnetic contribution to the phase

Since magnetic phase information is of primary interest in the present study, φ_M has to be separated from φ_E, especially close to the FeGe specimen edge, where the sample thickness and composition can change rapidly. Figure S7 illustrates the experimental procedure that was used here to separate the magnetic contribution to the phase shift using off-axis electron holography. Figure S7(a) shows the total phase shift recorded using off-axis EH from part of an FeGe lamella examined in an applied magnetic field $\mu_0 H$ of $\sim$ 100 mT at a temperature T $\sim$95 K. The spotty contrast features are associated with the formation of individual magnetic skyrmions. However, the dominant contrast arises from the electrostatic contribution to the phase shift φ_E and hinders the interpretation of the detailed skyrmion structure. We therefore subtracted the electrostatic contribution to the phase shift φ_E (Fig. S7(b)) from the total phase shift φ_{EM} (Fig. S7(a)) to obtain only the magnetic contribution to the phase shift φ_M (Fig. S7c). The electrostatic contribution to the phase shift φ_E shown in Fig. S7(b) was recorded at room temperature, well above the Curie temperature (T_C $\sim$280 K) of FeGe, at which the magnetic contribution to the phase shift is zero. This approach assumes that there is no change in diffraction contrast or mean inner potential with temperature.

2.3 Color-contour representaions of the projected in-plane magnetic induction

Magnetic induction maps were generated from the recorded magnetic contribution to the phase shift, both using phase contour lines and using colors to represent the directions and magnitudes of the measured projected in-plane magnetic induction. Figure S7(d) shows an example of a composite color-contour representation of the measured magnetic induction. Note that only the projected in-plane magnetic induction inside the specimen is shown in the present images, while the very weak fields outside the boundary of the specimen are masked out.

2.4 Model-based iterative magnetization reconstruction

A model-based approach was used to reconstruct the projected in-plane magnetization distribution from magnetic phase images recorded using off-axis electron holography. Figure S8(a) describes both the forward model and the inverse problem of magnetization reconstruction from an experimentally measured magnetic phase image.

Briefly, a mask is applied to outline the edge of the specimen, and an appropriate initial guess is made for the magnetization distribution $M(x, y)$ in the specimen on a two-dimensional Cartesian gird. A simulated magnetic phase image $\varphi(x, y)$ is then

calculated from $M(x, y)$. We make use of known analytical solutions for the phase shifts of simple geometrical objects, with numerical discretization performed in real space to avoid artifacts generated by discretization in Fourier space. This forward simulation approach is used in an iterative scheme to solve the inverse problem of reconstructing the projected in-plane magnetization distribution in the specimen from a two-dimensional phase image, as shown in Fig. S8(b). This approach allows additional physical constraints to be incorporated, such as the fact that the angles between the magnetic moments of adjacent discretized cells cannot be greater than a certain value. It should be noted that the sizes of the discretized cells should be smaller than the exchange length of the magnetic material.

3 LM video

We recorded sequences of LM images in real time during the application of varying temperatures or magnetic fields, and compiled them into videos.

3.1 Video 1: temperature of 240 K and varying field

In order to monitor magnetic transitions from zero-field helices to low-field skyrmions and high-field conical and ferromagnetic states, we recorded a video of Lorentz images (400 μm under focus) while varying the applied magnetic field normal to the specimen

plane from 0 to 200 mT over 274.1 seconds with a time step of 1.28 second per frame. The rate of change of the applied field was approximately 0.73 mT per second. The specimen temperature was stabilized at 240±0.1 K. In zero field, two grains supported magnetic helices. Upon increasing the field, the helices fluctuated and collectively adjusted their morphologies and positions. At an applied field of $\sim$ 60 mT, the stripy contrast transformed into spotty contrast at the edges of the grains, signifying skyrmion nucleation. On increasing the field, the helices gradually transformed into skyrmion lattices. The skyrmions then decreased in size, adjusted their positions and some of them collapsed on further increasing the field. At an applied field of 190 mT, the skyrmions had all collapsed into either a conical or a field-polarized ferromagnetic state. The video was recorded continuously up to an applied field of 200 mT. The field of view was 3690×2030 nm^2 over an image grid of 450×250 pixels.

In the video, it was observed that skyrmion nucleation in the grain boundary region depended strongly on the orientation of the helices relative to the grain boundary. Skyrmions nucleated first on increasing the field for a helix with a propagation vector that was oriented parallel to the grain boundary.

3.2 Video 2: applied field of 100 mT and varying temperature

In order to assess the effect of temperature on skyrmion formation, a video of Lorentz images ($400\mu m$ under focus) was recorded while varying the specimen temperature from 220 to 240 K over 961 seconds with a time step of 0.48 second per frame. The rate of change of the specimen temperate was $\sim$ 0.02 K per second. The specimen was imaged in an applied out-of-plane field of 100 mT. At 220 K and under 100 mT, the left hand grain was observed to be in a helical state while the right hand grain supported a skyrmion lattice. Upon increasing the temperature, the trapped metastable helices transformed into a skyrmion lattice. At a temperature of 235 K, skyrmions nucleated at the edge of the specimen and rapidly spread across the whole grain. It is noteworthy that the two grains have different crystallograhic orientations, as shown in Figs. S2(b) and (c).

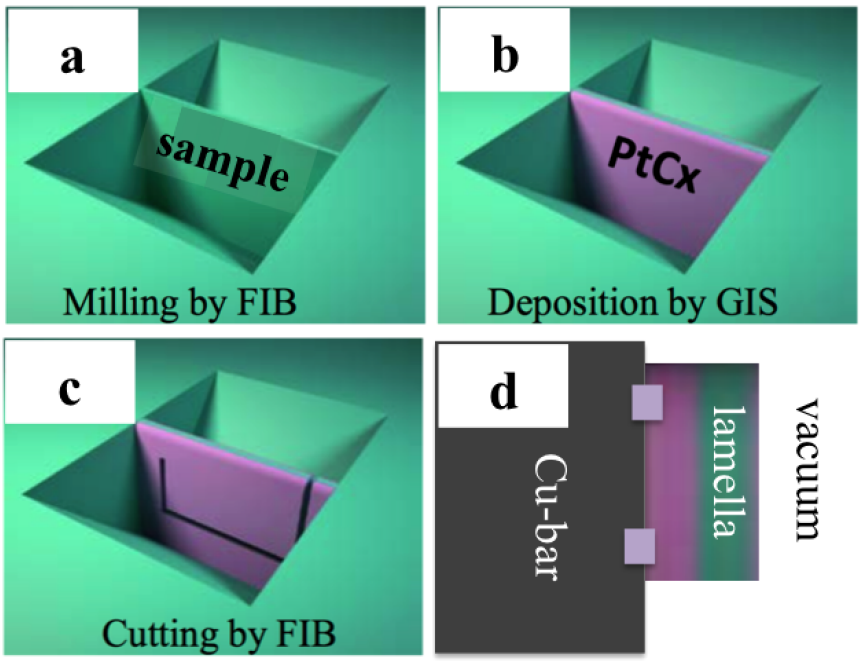

Figure S1: Schematic diagram describing the focused ion beam (FIB) milling and lift-out method. (a) FIB milling of an FeGe bulk sample. (b) Deposition of a Pt-C composite onto the specimen as a protective layer using a gas ion system (GIS). (c) FIB cutting of a thin lamella. (d) Lifting out and fixing the lamella onto a Cu bar using a lift-out method.

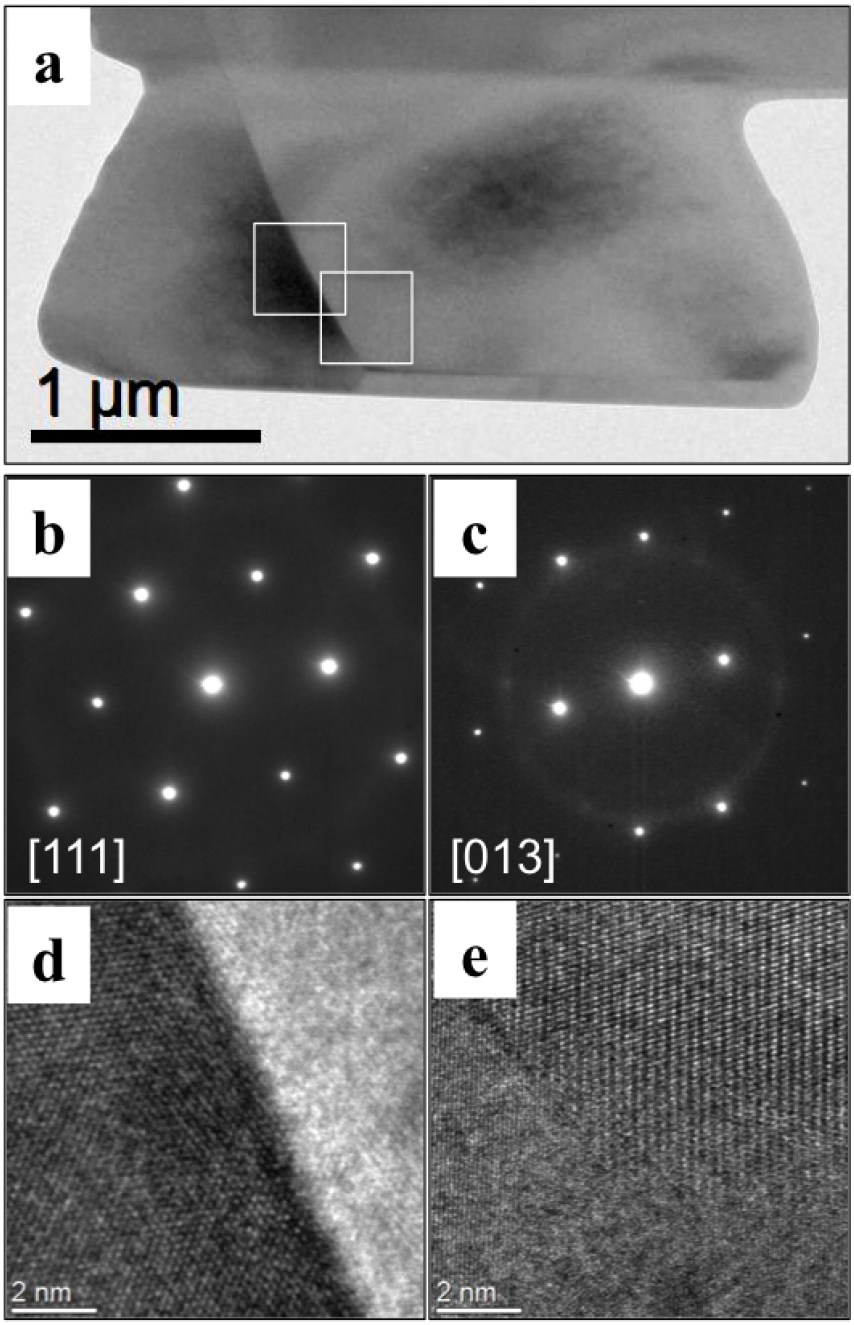

Figure S2: Structural characterization of an FeGe lamella. (a) Bright-field TEM image. (b) and (c) are electron diffraction patterns taken from the left and right hand grains in (a), respectively. (d) and (e) are high-resolution lattice images taken from the areas marked in (a).

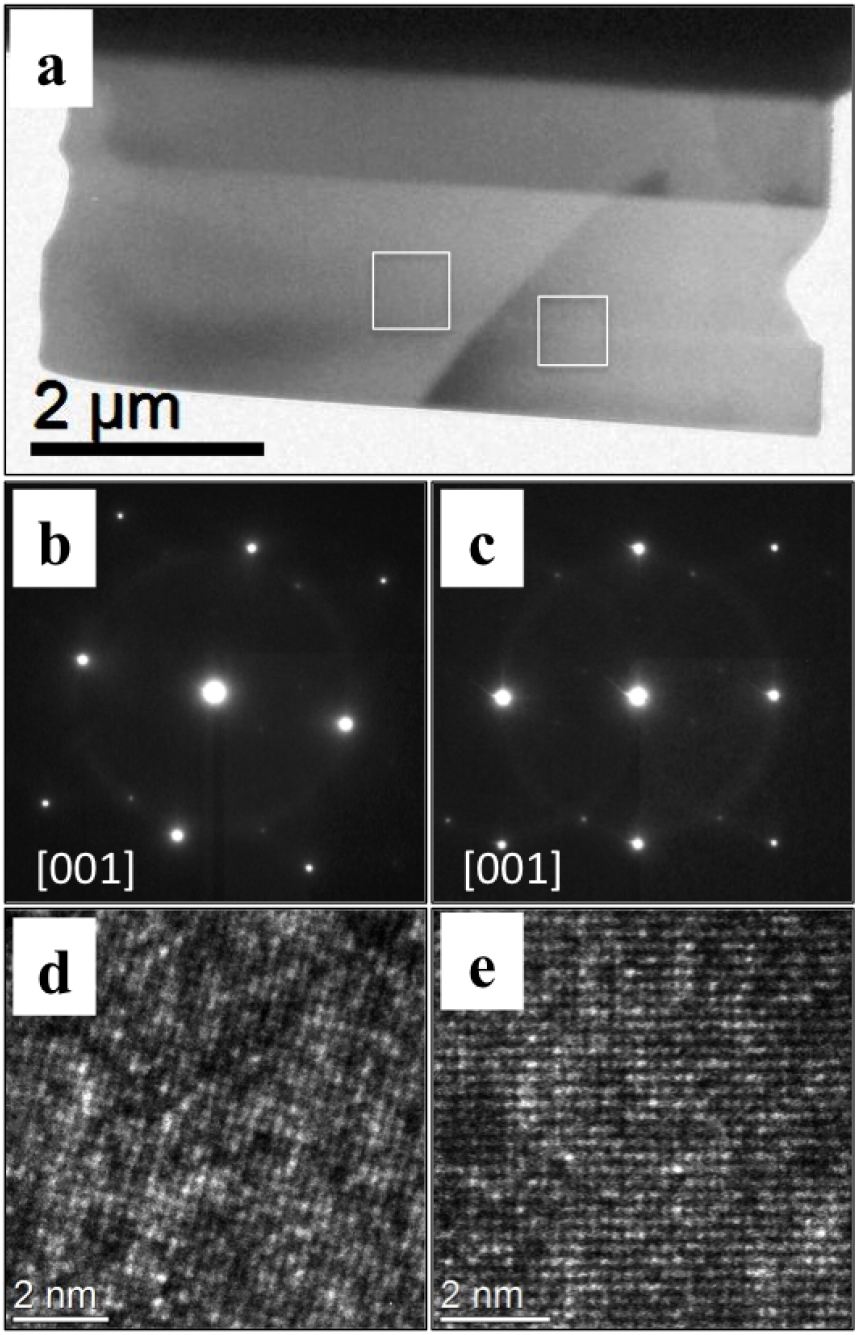

Figure S3: Structural characterization of an FeGe lamella. (a) Bright-field TEM image. (b) and (c) are electron diffraction patterns taken from the left and right hand grains in (a), respectively. (d) and (e) are high-resolution lattice images taken from the areas marked in (a).

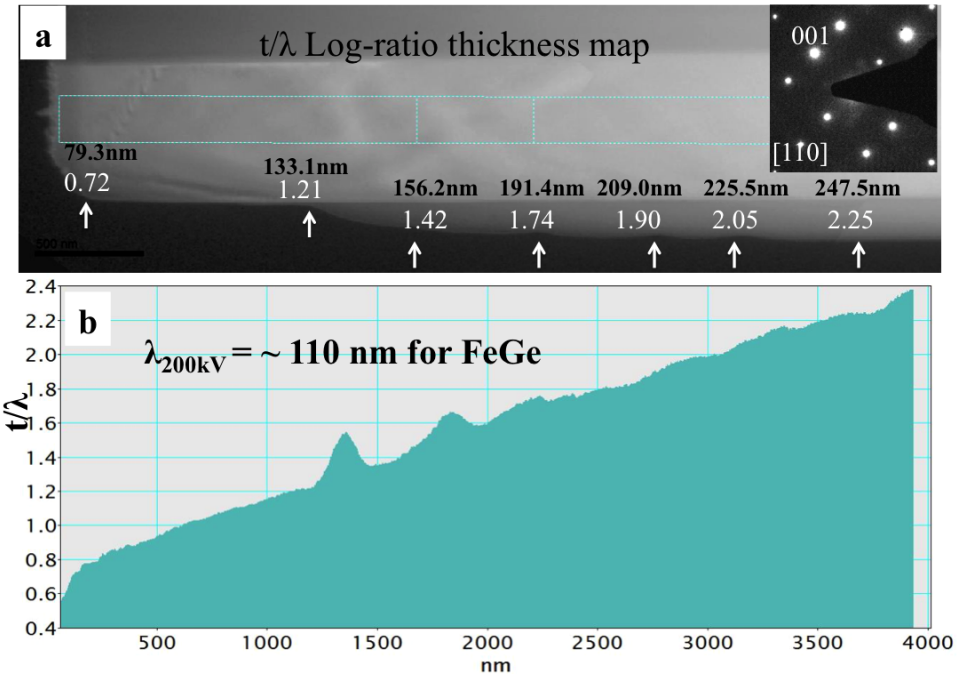

Figure S4: Structure and thickness map of an FeGe nanostripe. (a) Thickness map of an FeGe nanostripe measured by a log-ratio method using electron energy-loss spectroscopy. Inset is an electron diffraction pattern recorded from the nanostripe. (b) Line profile extracted from the region indicated in (a).

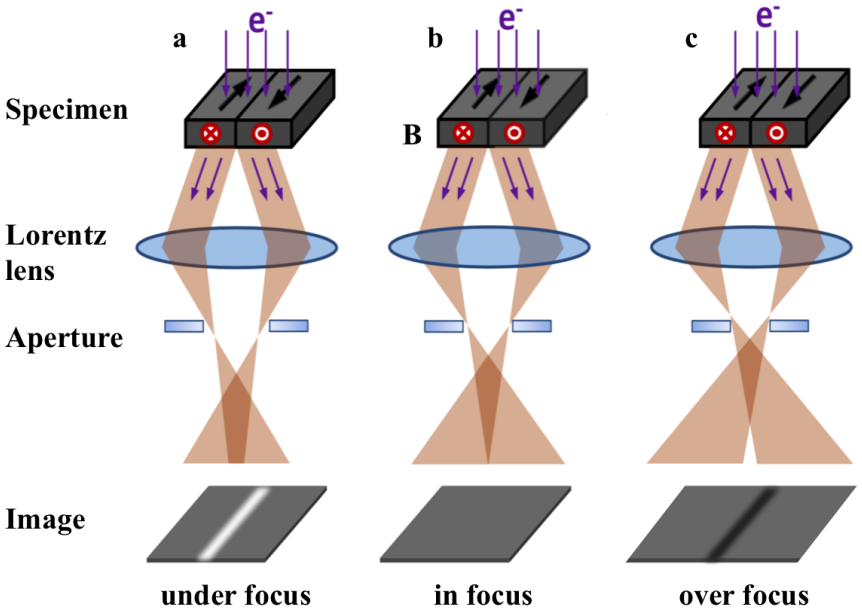

Figure S5: Schematic ray diagrams showing Fresnel imaging of 180° magnetic domains. Magnetically deflected electron beams from two oppositely magnetized domains (a) converge under focus and (c) diverge over focus conditions at the domain wall region. (b) In focus, the deflected beams are focused onto the image plane and no magnetic contrast is seen.

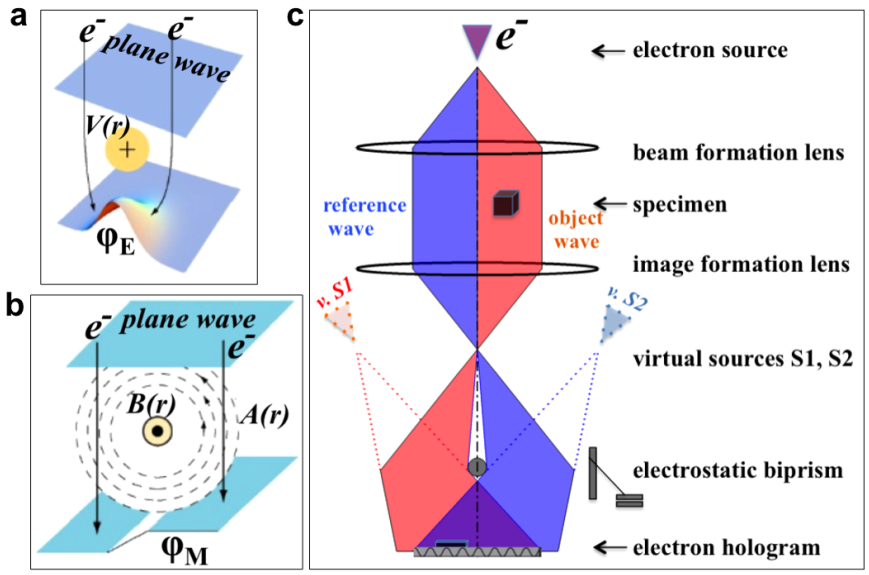

Figure S6: Schematic diagrams showing different contributions to the electron-optical phase shift arising from local variations in electrostatic scalar potential and magnetic vector potential measured using off-axis electron holography. (a) Electrostatic phase contribution φ_E originating from the electrostatic potential $V(r)$ within and around a TEM specimen. (b) Magnetic phase contribution φ_M originating from the magnetic vector potential $A(r)$ within and around a TEM specimen. (c) Simplified ray diagram for off-axis electron holography. Essential components are a coherent electron source, electromagnetic lenses and an electrostatic biprism for separation and overlap of the two parts of the electron wave to form an electron hologram. The object and reference waves can be considered as originating from two virtual sources $S1$ and $S2$. The electron-transparent specimen occupies approximately half of the field of view. For recording information about the magnetic properties of the specimen, the conventional TEM objective lens is normally switched off and a non-immersion Lorentz lens is used as the primary imaging lens. A pre-calibrated magnetic field can then be applied to the specimen in the electron beam direction by exciting the conventional objective lens slightly. Electron holograms can be recorded digitally for further analysis to yield information about the projected electromagnetic potential within and around the specimen.

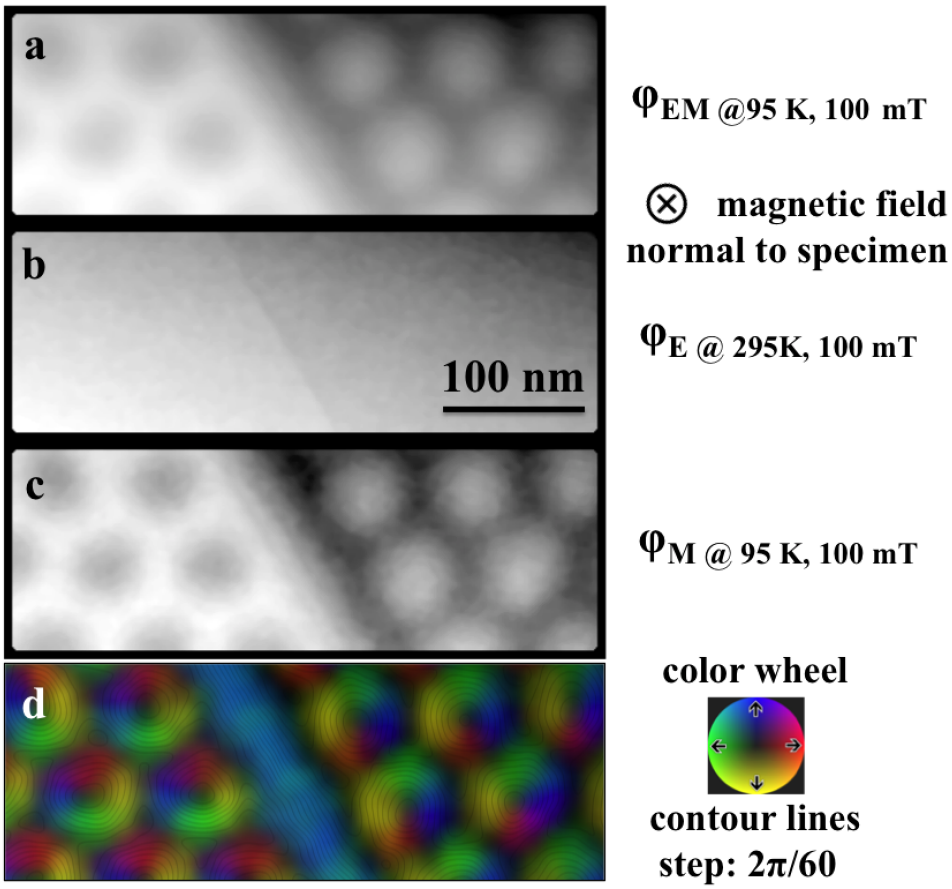

Figure S7: Procedure for separation of the electrostatic and magnetic contributions to the phase. (a) Total phase φ_{EM} acquired at 95 K in an applied field of 100 mT. (b) Electrostatic phase φ_E acquired at 295 K in field of 100 mT. (c) Magnetic phase φ_M obtained by subtracting φ_E from φ_{EM}. (d) Color-contour map of the projected in-plane magnetic induction. The hue represents the direction of the projected magentic induction according to the color wheel (red = right, yellow = down, green = left, blue = up). The contour lines have a spacing of $2\pi/60$ radians.

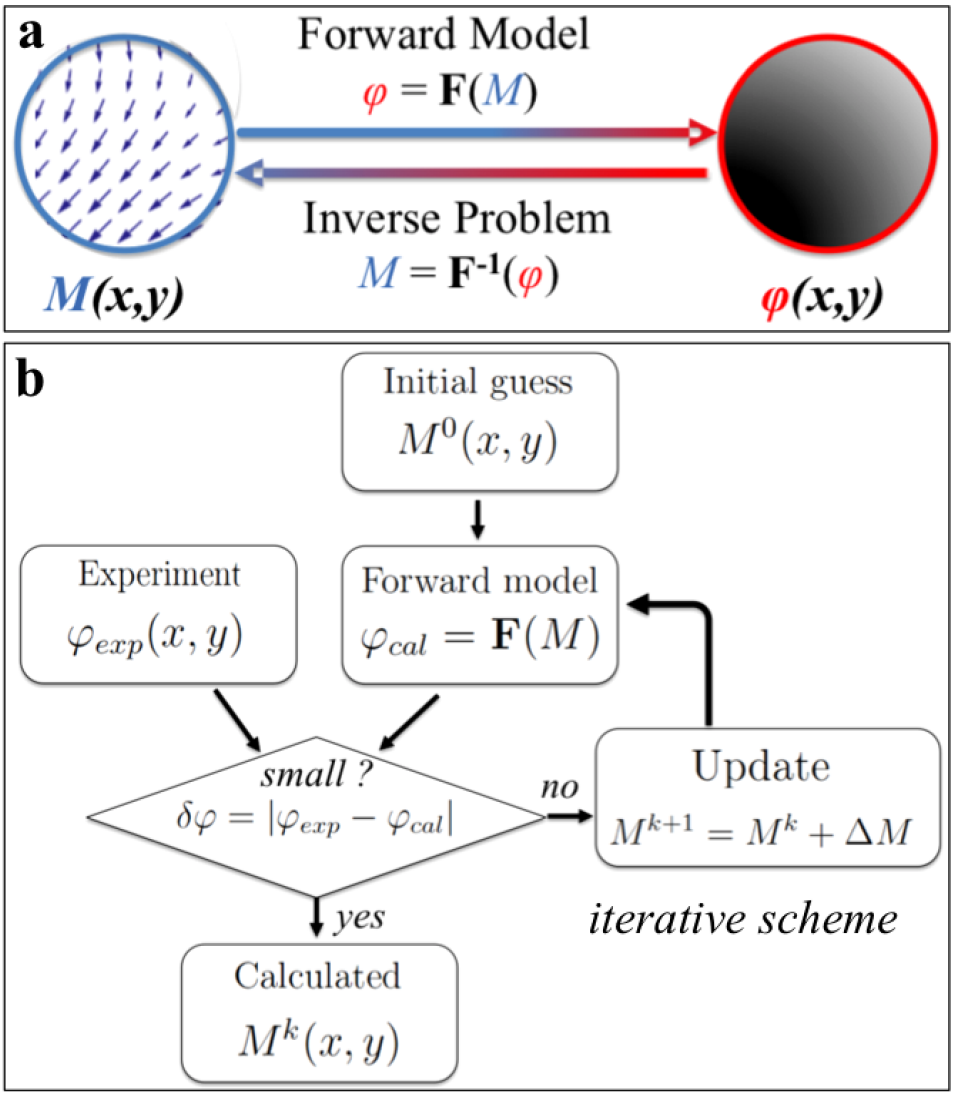

Figure S8: Description of the model-based iterative magnetization reconstruction algorithm used in the present study. (a) Forward model and inverse problem. (b) Flow chart illustrating the iterative reconstruction of the projected in-plane magnetization from an experimental magnetic phase image.